International Forum on Aeroelasticity and Structural Dynamics
IFASD 2017
25-28 June 2017 Como, Italy

FLIGHT FLUTTER TESTING USING HIGHER ORDER DYNAMIC MODE DECOMPOSITION

Rubén Moreno-Ramos[1], Soledad Le Clainche[2], José M. Vega[2], Paul F. Taylor[3]

[1]Altran Innovación, Aeronautics Space and Defence Division
C/ Campezo, 1, E-28022, Madrid, Spain
ruben.morenoramos@altran.com

[2]E.T.S.I. Aeronáutica y del Espacio, Universidad Politécnica de Madrid
Pza. Cardenal Cisneros, E-28040, Madrid, Spain

[3]Gulfstream Aerospace Corporation
Savannah, Georgia, 31402, USA

Keywords: Flutter Testing, ARMA, DMD

Abstract: This paper presents the application of higher order dynamic mode decomposition (HODMD) to flutter flight test data in order to extract aircraft frequencies and damping. The method is an extension of DMD, a method typically used to extract flow patterns and frequencies from unsteady fluid dynamics measurements or simulations. In the fluid dynamics field, it has been shown to be able to extract modes, frequencies and damping from very noisy and large signals, in a robust and efficient way, with reduced manual interaction.

1 INTRODUCTION

Flight flutter testing is a requirement for civil transport category aircraft certified in the United States under the Code of Federal Regulations, Part 25. Flight flutter testing often involves taking the aircraft to parts of the flight envelope it has not been to prior and performing stability checks at those points.

Normal flight clearance typically involves flying very fast at a broad range of altitudes, including multiple fuel and payload configurations, meaning that the testing can be very expensive in terms of both fuel and time. This places an emphasis on efficient testing techniques, including test point sequencing, piloting techniques and near real time data reduction and modal parameter extraction techniques.

The execution of the flight flutter testing consists on mounting on the aircraft an array of accelerometers that measure the structural dynamics response to several inputs coming from the control surfaces or any mounted flutter excitation system (FES). Accelerometer responses together with some other type of data extracted from the flight, such as control surface displacements for pulses or control surface sweeps, force measurements from the FES and flight parameters, are stored with the aim of analyzing them. The main goal is to obtain the aircraft damping rates ζ_m and frequencies ω_m that are related to the flutter phenomenon. The computational resources required within this data acquisition process and analysis are directly linked to both the quantity of data stored (memory) and the time employed in the damping/frequency calculations

(computational time). These two issues are highly dependent on the numerical method used for the analysis.

Several methods for the damping, frequency and mode shapes extraction are presented in the literature such as, moving-block approach (MBA) [1], least-squares curve-fitting method (LSCFM) [2], auto-regressive moving-average method (ARMA) [3, 4], some advanced signal processing techniques [5], etcetera. McNamara & Friedman [6] have shown the ARMA method to be highly efficient and effective, leading to the reduction of computational cost in both, memory and time. This aspect makes ARMA suitable for performing damping/frequency analysis in flight flutter testing. The method, as presented by McNamara & Friedman [6], assumes that there is a linear relationship between the state $\tilde{\mathbf{X}}_k$ (at time instant t_k) and subsequent state $\tilde{\mathbf{X}}_{k+1}$ (at time instant t_{k+1}). Such linear relationship is independent of k, and may be represented by a matrix whose eigenvalues determine the frequencies and damping rates of the system.

There is a tight link between the ARMA method and dynamic mode decomposition (DMD) [7], a method commonly used in fluid dynamics to study the frequencies and damping rates (also known as growth rates) of a flow system. The standard DMD algorithm is based on the Koopman assumption [8], which relates each snapshot (state vector) with the subsequent snapshot via the linear operator $\mathbf{R}$ as

$$\mathbf{X}_{k+1} \simeq \mathbf{R}\mathbf{X}_k \quad \text{for } k = 1, \ldots, K-1. \tag{1}$$

When the snapshots are organized in snapshots matrices of the form

$$\boldsymbol{X}_p^Q = [\boldsymbol{x}_p, \boldsymbol{x}_{p+1}, \ldots, \boldsymbol{x}_k, \boldsymbol{x}_{k+1}, \ldots, \boldsymbol{x}_{Q-1}, \boldsymbol{v}_Q] \tag{2}$$

equation (1) can also be written as

$$\mathbf{X}_2^K \simeq \mathbf{R}\mathbf{X}_1^{K-1} \simeq \mathbf{X}_1^{K-1}\mathbf{C}, \tag{3}$$

where $\mathbf{C}$ is a companion matrix. The dynamics of the system (damping rates and frequencies) are determined from the eigenvalues of either $\mathbf{R}$ or $\mathbf{C}$, as in the ARMA method. When DMD analysis is performed via the linear operator $\mathbf{R}$ instead of the companion matrix, the results are improved, since, as it will be explained in Section 2, it is possible to remove spatial redundancies (too many samples) or to clean their noise.

It is remarkable the similarity between ARMA and DMD algorithm, since both algorithms relate subsequent vector states by a companion matrix. The differences found between these two methods lie in the generation of the vector state, in each case ordered in different ways, and consequently, the coefficients and the structure of the companion matrix are also different. The companion matrix is defined in the ARMA method as

$$\tilde{\mathbf{C}} \equiv \begin{bmatrix} -\boldsymbol{a}_1 & \underline{1} & \mathbf{0} & \ldots & \mathbf{0} \\ -\boldsymbol{a}_2 & \mathbf{0} & \underline{1} & \ldots & \mathbf{0} \\ \ldots & \ldots & \ldots & \ldots & \ldots \\ -\boldsymbol{a}_{K-1} & \mathbf{0} & \mathbf{0} & \ldots & \underline{1} \\ -\boldsymbol{a}_K & \mathbf{0} & \mathbf{0} & \ldots & \mathbf{0} \end{bmatrix}. \tag{4}$$

while in standard DMD it is defined as

$$\boldsymbol{C} \equiv \begin{bmatrix} \mathbf{0} & \mathbf{0} & \dots & \mathbf{0} & \boldsymbol{c}_1 \\ \underline{1} & \mathbf{0} & \dots & \mathbf{0} & \boldsymbol{c}_2 \\ \mathbf{0} & \underline{1} & \dots & \mathbf{0} & \boldsymbol{c}_3 \\ \dots & \dots & \dots & \dots & \dots \\ \mathbf{0} & \mathbf{0} & \dots & \underline{1} & \boldsymbol{c}_K \end{bmatrix}. \tag{5}$$

where $\boldsymbol{a}_1, \cdots, \boldsymbol{a}_K$ and $\boldsymbol{c}_1, \cdots, \boldsymbol{c}_K$ are the coefficients calculated for each companion matrix. Since the state vector contains relevant temporal information, the essence of these two algorithms is, however, the same. Thus, different distributions of each one of the components of the state vector would vary the coefficients of the companion matrix but would provide the same results. It is important to mention that, to obtain consistent results in both ARMA and standard DMD, it is necessary to maintain the same order of the state vector components at each time instant (columns of the sate vector).

In temporal signals, it is possible to decompose the original data $\mathbf{x}_k$ ($\mathbf{x}_k$ represents each one of the state variables) as an expansion of M Fourier-like modes in the following way

$$\mathbf{x}_k \simeq \mathbf{x}_k^{approx.} \equiv \sum_{m=1}^{M} a_m \mathbf{u_m} e^{(\zeta_m + i\omega_m)(k-1)\Delta t}, \quad k = 1, \dots, K, \tag{6}$$

where the number of terms M, can be referred to as the *spectral complexity*, $K \leq n$ is the *temporal dimension*, $\mathbf{u_m}$ are the spatial coefficients or modes (unitary vector) and a_m are their corresponding amplitudes. The dimension of the subspace generated by the M modes is the *spatial complexity* N.

Using standard DMD algorithm, not only the damping rates and frequencies are easily obtained, but also the associated spatial modes and their corresponding amplitudes. The benefits of DMD have been put in evidence several times in the literature [9–11]. However, the method does not always give the expected results when the signal (or flow) studied is noisy and complex [12], or when the spatial complexity N is smaller than the spectral complexity M. Therefore, Le Clainche & Vega [13] proposed an extended algorithm, called higher order dynamic mode decomposition (HODMD), in order to address such problems. The method, similarly to ARMA or standard DMD, is highly effective in terms of computational cost. Additionally, it has been shown to provide more accurate results with a shorter length signal than DMD (see Figure 5.1 in [13]). In this article, this new method is applied to a set of experimental flight flutter testing data, obtained during a flutter flight test campaign, and its good performance is put in evidence. Three different flight test points have been analyzed.

2 HIGHER ORDER DYNAMIC MODE DECOMPOSITION

The main goal of HODMD is to express a set of instantaneous (spatio-temporal) data as an expansion of modes as shown in equation (6), thus it is possible to study the main frequencies and growth rates composing a signal. For convenience, a set of K time equispaced snapshots obtained in a flight test (the signal of an accelerometer) are collected in the following matrix

$$\boldsymbol{V}_1^K = [\boldsymbol{v}_1, \boldsymbol{v}_2, \dots, \boldsymbol{v}_k, \boldsymbol{v}_{k+1}, \dots, \boldsymbol{v}_{K-1}, \boldsymbol{v}_K], \tag{7}$$

where each vector $\boldsymbol{v}_k$ is composed by the signal at time instant t_k collected in each one of the accelerometers of the flight test. Then, the HODMD algorithm proceeds in two main steps.

- *Step 1: Dimension reduction.* In a first step, the spatial dimension J (number of accelerometers) of the original data set of snapshots is reduced to a set of linearly dependent vectors of dimension N, reducing the noise of the signal. In this way, singular value decomposition [14] (SVD) is applied to the snapshots matrix as

$$\boldsymbol{V}_1^K \simeq \boldsymbol{W}\,\boldsymbol{\Sigma}\,\boldsymbol{T}^\top, \tag{8}$$

where $\boldsymbol{W}^T\boldsymbol{W} = \boldsymbol{T}^T\boldsymbol{T} =$ the $N \times N$ unit matrix and the diagonal of matrix $\boldsymbol{\Sigma}$ contains the singular values $\sigma_1, \cdots, \sigma_K$. The number of retained SVD modes, N, is calculated through the standard SVD-error estimated for a certain tolerance ε (set by the user) as

$$\frac{\sigma_{N+1}^2 + \cdots + \sigma_K}{\sigma_1^2 + \cdots + \sigma_K} \leq \varepsilon. \tag{9}$$

Then the *reduced snapshots matrix* of dimension $N \times K$ is written as

$$\hat{\boldsymbol{V}}_1^K = \boldsymbol{\Sigma}\,\boldsymbol{T}^\top, \quad \text{with } \boldsymbol{V}_1^K = \boldsymbol{W}\hat{\boldsymbol{V}}_1^K \tag{10}$$

- *Step 2: DMD-d.* The following higher order Koopman assumption (written in matrix form)

$$\boldsymbol{V}_{d+1}^K \simeq \boldsymbol{R}_1\boldsymbol{V}_1^{K-d} + \boldsymbol{R}_2\boldsymbol{V}_2^{K-(d-1)} + \ldots + \boldsymbol{R}_d\boldsymbol{V}_d^{K-1}. \tag{11}$$

is applied to the reduced snapshots matrix. Pre-multiplying (11) by $\boldsymbol{W}^\top$, where the *reduced Koopman operator* yields $\hat{\boldsymbol{R}}_k = \boldsymbol{W}^T\boldsymbol{R}_k\boldsymbol{W}$, one leads to the following expression

$$\hat{\boldsymbol{V}}_{d+1}^K \simeq \hat{\boldsymbol{R}}_1\hat{\boldsymbol{V}}_1^{K-d} + \hat{\boldsymbol{R}}_2\hat{\boldsymbol{V}}_2^{K-d+1} + \ldots + \hat{\boldsymbol{R}}_d\hat{\boldsymbol{V}}_d^{K-1}. \tag{12}$$

The main system dynamics (frequencies, damping rates and DMD modes) are contained in all these linear operators that can be encompased in the *modified Koopman matrix* (that contains the dynamics of the system) of dimension $Nd \times Nd$, defined as

$$\tilde{\boldsymbol{R}} \equiv \begin{bmatrix} \mathbf{0} & \mathbf{I} & \mathbf{0} & \ldots & \mathbf{0} & \mathbf{0} \\ \mathbf{0} & \mathbf{0} & \mathbf{I} & \ldots & \mathbf{0} & \mathbf{0} \\ \ldots & \ldots & \ldots & \ldots & \ldots & \ldots \\ \mathbf{0} & \mathbf{0} & \mathbf{0} & \ldots & \mathbf{I} & \mathbf{0} \\ \hat{\boldsymbol{R}}_1 & \hat{\boldsymbol{R}}_2 & \hat{\boldsymbol{R}}_3 & \ldots & \hat{\boldsymbol{R}}_{d-1} & \hat{\boldsymbol{R}}_d \end{bmatrix}. \tag{13}$$

Using a *modified reduced snapshot matrix*, it is possible to write a more general higher order Koopman assumption as

$$\tilde{\boldsymbol{V}}_2^{K-d} = \tilde{\boldsymbol{R}}\,\tilde{\boldsymbol{V}}_1^{K-d+1}. \tag{14}$$

In a first step, as in the standard DMD algorithm (or ARMA), the modified Koopman matrix is calculated. Next, the eigenvalue problem of such matrix is solved. The eigenvalues obtained give the frequencies and damping rates of the DMD expansion (6), and the eigenvectors are used to calculate the DMD modes $\boldsymbol{u}_m$. Finally, the amplitudes related to each mode are calculated using a least squares fitting. A second tolerance ε_1 is

set by the user to retain the most relevant DMD modes, as a function of their amplitudes. A more detailed description of this algorithm is presented in the literature [13].
The parameter d identified in equation (11) is set by the user after some calibration, looking for robustness of the results (similar results for different d and Δt) [12]. It is remarkable that if $d = 1$, the algorithm is similar to standard DMD algorithm, formulated in equation (1). Thus, when standard DMD succeeds HODMD provides the same results (for values of d≥ 1), and in the case that it fails (noisy or transient flows) it improves its performance.

After the HODMD calculation has been performed, it is possible to reconstruct the original results using the general DMD expansion of equation (6). Thus, in cases in which the results are very noisy and complex (a signal defined by a large number of frequencies), it is possible to improve the performance of HODMD using the method iteratively [12]. Once HODMD is applied to the original data, it is reconstructed as in (6). Then, it is possible to apply HODMD to the reconstructed data, obtaining a new DMD expansion, and so on. The iterative HODMD method is the one that has been used for the present analysis.

Since the data analyzed is very noisy and complex, the data presented in the snapshots matrix (7) is transformed using the auto-correlation matrix [5]. Then, the HODMD algorithm is applied to the part corresponding to the positive lags of the correlation matrix. In this way, the data is cleaner, and consequently the dominant frequencies are more accurate. However, the calculated damping rates are modified. The results (frequencies) obtained using the auto-correlation matrix are also shown in this article, and they are used to estimate the value of the frequency in the analysis using the raw data.

3 RESULTS

HODMD has been applied to a set of data coming from real aircraft flutter flight testing with the aim of calculating the most relevant frequencies, damping rates and their associated mode shapes. Three different flight test have been carried out, using 92 accelerometers, which represent the spatial complexity $J = N$ of the system. The number of snapshots used for this analysis is $K = 4301$ (of a total number of 21508 samples), equispaced in time Δt. On the one hand, as mentioned before, classical methods fail in the damping/frequency calculations if $N < M$. For example, if the signal is too complex (a large number of frequencies and damping rates $M >> N$) or if the number of accelerometers is too low ($N << M$). Thus, HODMD seems a suitable choice to perform this analysis. On the other hand, DMD algorithm using companion matrix (or ARMA) would make profit of the spatial redundancies of the data (the companion matrix is based on the linear dependence of the data) [15], and they might capture the most relevant frequency, but with smaller accuracy, and some of the results also might be misunderstood [12]. HODMD cleans the spectra from noise and captures more than a single relevant frequency.

HODMD is based on the robustness of the results, thus if the method is applied to the same data set at different time instants, using different time intervals, d or ε, ε_1, the same results are obtained. To illustrate the method, HODMD has been applied to the output of the 92 accelerometers of the first flight test of a flutter flight test campaign, using either the original raw data or the positive lags of the auto-correlation matrix and different test parameters, d, ε, ε_1.

Figure 1 shows the results obtained for this analysis. As it can be seen, in all cases it is possible to identify clearly 6 peaks, related to different frequencies. The amplitude of 4 of these peaks is

large, and they are very well defined in the spectrum (straight vertical line that defines ω_1, ω_2, ω_3 and ω_4). However, the amplitude of the frequency related to the 2 remaining peaks (ω_5 and ω_6) is smaller, and these frequencies are more mixed with the spurious modes, related to the noise of the signal.

Table 1 shows the value of the frequency and damping rate of the highest amplitude mode in each of the vertical lines shown in Figure 1. The data is obtained in the three test iterations by applying HODMD to the time data (not the auto-correlation). As it can be seen, the results are consistent and robust. Similar frequencies and growth rates are obtained in the three cases. However, there is a slight inconsistency in test cases T2 and T1 in the calculations of the damping rates related to ω_5 and ω_6, respectively. As previously mentioned, these are lower amplitude frequencies, mixed with noise. Thus, to calculate these modes (to improve the data cleaning), it is necessary to use smaller tolerances ($\varepsilon = \varepsilon_1 < 5 \cdot 10^{-3}$) and larger values of d ($d > 500$), as seen in T3.

Figure 2 shows the modes related to the four highest amplitude frequencies ω_1, ω_2, ω_3 and ω_4. Real and imaginary part of DMD modes alternate every semi period (of the frequency captured) in time (π). The module of the mode gives an idea of where the main activity (sensor activity) is focused. The modes with highest value represent the sensor that is relevant for capturing such frequency. Figure 3 shows DMD modes whose absolute value is larger than one. As it can be seen, only a few sensors ($\sim$ 30 from 92) are related to these frequencies, thus with a smaller number of sensors, located at some specific places, it would be possible to obtain the same solution.

Following the same methodology, HODMD has been performed for the two remaining flight test. Figure 4 shows the evolution of each of the three highest amplitude frequencies and damping rates as function of the test case.

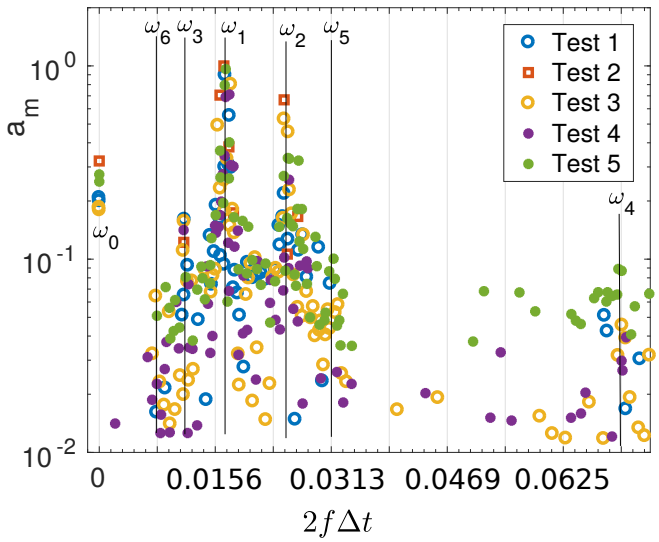

Figure 1: Spectrum of frequencies and aplitudes obtained unsing HODMD and different tolerances (ε, ε_1) and d, in the first flight test.

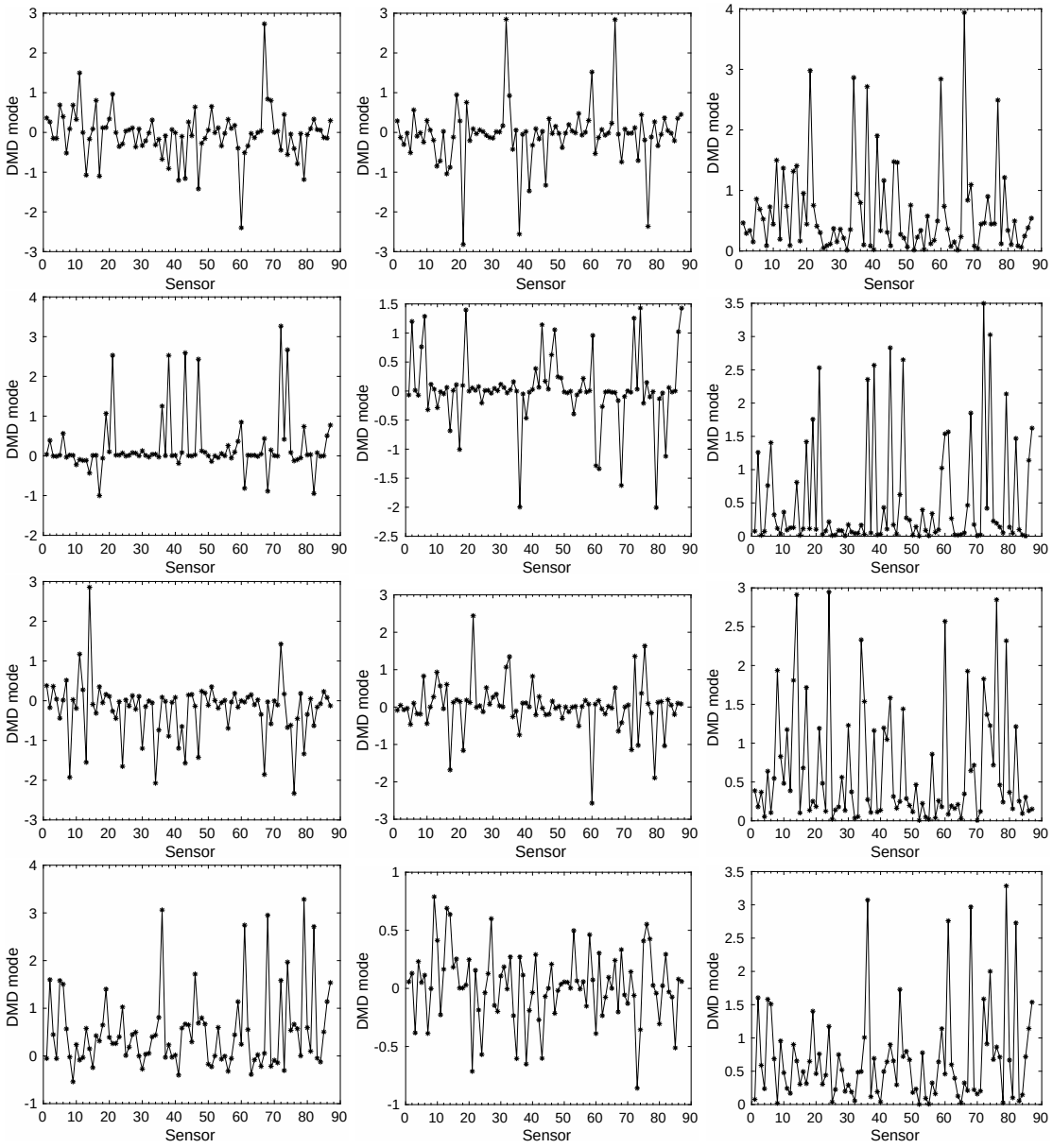

Figure 2: DMD modes in each one of the 92 sensors for the first flight test. From left to right: real part, imaginary part and module. From top to bottom: DMD modes of ω_1, ω_2, ω_3 and ω_4.

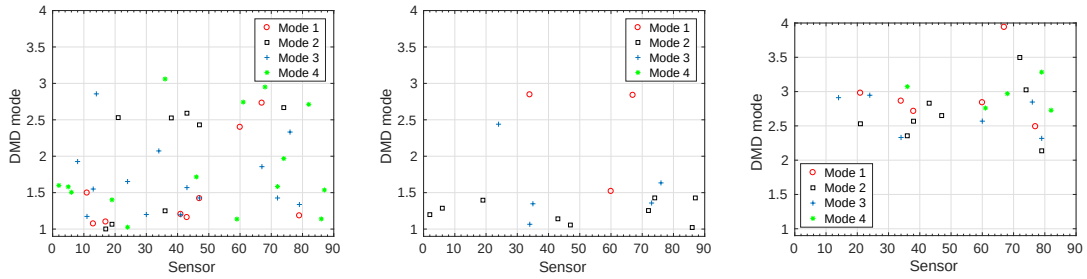

Figure 3: Four highest amplitude DMD modes, with absolute value larger than 1 for the real and imaginary part (left and middle), and with absolute values larger than 2 for the module (right).

	$2f\Delta t$	ζ
T1	0.0169	0.02
T2	0.0169	0.02
T3	0.0170	0.03
T1	0.0255	0.075
T2	0.0248	0.08
T3	0.0253	0.06
T1	0.0113	0.05
T2	0.0122	0.044
T3	0.0116	0.05
T1	0.0704	0.02
T2	0.0705	0.03
T3	0.0703	0.025
T1	0.0270	*0.08*
T2	0.0266	0.027
T3	0.0267	0.03
T1	0.0077	0.015
T2	0.0077	*0.08*
T3	0.0077	0.017

Table 1: Frequencies and damping rates obtained using HODMD in the first fight test in with three different tolerances (ε, ε_1) and d, corresponding to the highes amplitude frequency of each frequency group shown in Figure 1. From top to bottom: ω_1, ω_2, ω_3, ω_4, ω_5 and ω_6.

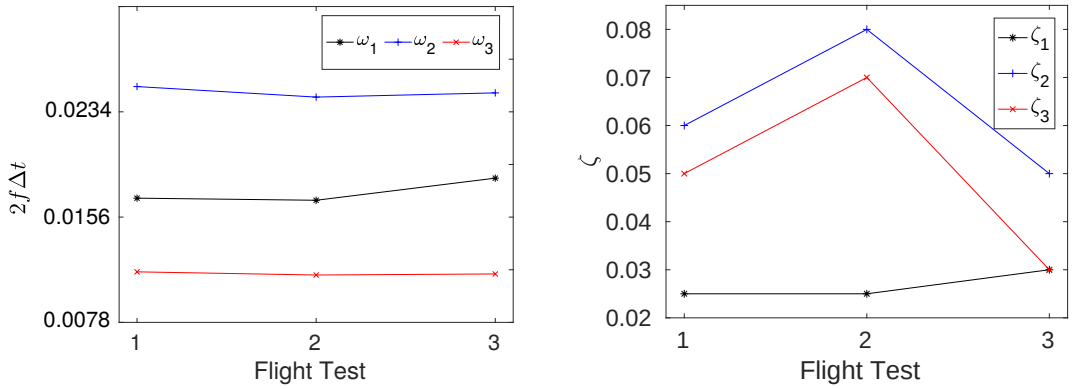

Figure 4: Frequency (left) and damping rate (right) variation in each one of the three flight test performed.

4 CONCLUSIONS AND FUTURE WORK

The application of the, recently developed, HODMD method to the extraction of aircraft modal characteristics from flutter flight testing data, has been presented in this paper. The method originates from the standard DMD (which is similar to the ARMA method) and improves it to be able to deal with higher spatial dimension, lower signal durations and higher signal to noise ratio.

The method has been able to extract, in a robust and efficient manner, the most relevant aircraft modes from test data in an operational sense, that is without making use of any known excitation.

The results are very promising, but the suitability of the method needs to be corroborated with the analysis of a higher number of test points, as well as the comparison of the results with data extracted using industry standard methods.

ACKNOWLEDGMENTS

This work was partially supported by the Spanish Ministry of Economy and Competitiveness, under grant TRA2016-75075-R.

5 REFERENCES

[1] Hammond, C. E. and Doggett, R. V., Jr. (1976). Determination of Subcritical Damping by Moving-Block Applications. In *Flutter Testing Techniques*, vol. 415 of *NASA Special Publication*. p. 59.

[2] Bennett, R. M. and Desmarais, R. N. (1976). Curve Fitting of Aeroelastic Transient Response Data with Exponential Functions. In *Flutter Testing Techniques*, vol. 415 of *NASA Special Publication*. p. 43.

[3] Matsuzaki, Y. and Ando, Y. (1981). Estimation of flutter boundary from random responses due to turbulence at subcritical speeds. *Journal of Aircraft*, 18(10), 862–868.

[4] Matsuzaki, Y. and Ando, Y. (1981). Estimation of flutter boundary from random responses due to turbulence at subcritical speeds. *Journal of Aircraft*, 18(10), 862–868.

[5] Taylor, P. F., Moreno, R., Banavara, N., et al. (2017). Flutter flight testing at gulfstream aerospace using advanced signal processing techniques. In *58th AIAA/ASCE/AHS/ASC Structures, Structural Dynamics, and Materials Conference*. p. 1823.

[6] McNamara, J. J. and Friedmann, P. P. (2007). Flutter boundary identification for time-domain computational aeroelasticity. *AIAA journal*, 45(7), 1546–1555.

[7] Schmid, P. J. (2010). Dynamic mode decomposition of numerical and experimental data. *Journal of fluid mechanics*, 656, 5–28.

[8] Koopman, B. O. (1931). Hamiltonian systems and transformation in hilbert space. *Proceedings of the National Academy of Sciences*, 17(5), 315–318.

[9] Le Clainche, S., Li, J. I., Theofilis, V., et al. (2015). Flow around a hemisphere-cylinder at high angle of attack and low reynolds number. part i: Experimental and numerical investigation. *Aerospace Science and Technology*, 44, 77–87.

[10] Le Clainche, S., Rodríguez, D., Theofilis, V., et al. (2015). Flow around a hemisphere-cylinder at high angle of attack and low reynolds number. part ii: Pod and dmd applied to reduced domains. *Aerospace Science and Technology*, 44, 88–100.

[11] Gómez, F., Clainche, S. L., Paredes, P., et al. (2012). Four decades of studying global linear instability: progress and challenges. *AIAA journal*, 50(12), 2731–2743.

[12] Le Clainche, S., Vega, J., and Soria, J. (2017). Higher order dynamic mode decomposition for noisy experimental data: flow structures on a zero-net-mass-flux jet. *Submitted to Exp. Therm. and Fluid Sci.*

[13] Le Clainche, S. and Vega, J. M. (2017). Higher order dynamic mode decomposition. *SIAM Journal on Applied Dynamical Systems*, 16(2), 882–925.

[14] Sirovich, L. (1987). Turbulence and the dynamics of coherent structures. parts i–iii. *Quarterly of applied mathematics*, 45(3), 561–571.

[15] Schmid, P. J. (2011). Application of the dynamic mode decomposition to experimental data. *Experiments in fluids*, 50(4), 1123–1130.

COPYRIGHT STATEMENT